

A Comparison of the Effect of Temperature on the Passivity Breakdown and Repassivation Potentials of Wrought and Welded Alloy 22 in 5 M CaCl₂

G.O. Ilevbare

This article was submitted to
203rd ECS Meeting, Paris, France, April 27 – May 2, 2003

February 14, 2003

U.S. Department of Energy

Lawrence
Livermore
National
Laboratory

DISCLAIMER

This document was prepared as an account of work sponsored by an agency of the United States Government. Neither the United States Government nor the University of California nor any of their employees, makes any warranty, express or implied, or assumes any legal liability or responsibility for the accuracy, completeness, or usefulness of any information, apparatus, product, or process disclosed, or represents that its use would not infringe privately owned rights. Reference herein to any specific commercial product, process, or service by trade name, trademark, manufacturer, or otherwise, does not necessarily constitute or imply its endorsement, recommendation, or favoring by the United States Government or the University of California. The views and opinions of authors expressed herein do not necessarily state or reflect those of the United States Government or the University of California, and shall not be used for advertising or product endorsement purposes.

This is a preprint of a paper intended for publication in a journal or proceedings. Since changes may be made before publication, this preprint is made available with the understanding that it will not be cited or reproduced without the permission of the author.

This report has been reproduced directly from the best available copy.

Available electronically at <http://www.doc.gov/bridge>

Available for a processing fee to U.S. Department of Energy
And its contractors in paper from
U.S. Department of Energy
Office of Scientific and Technical Information
P.O. Box 62
Oak Ridge, TN 37831-0062
Telephone: (865) 576-8401
Facsimile: (865) 576-5728
E-mail: reports@adonis.osti.gov

Available for the sale to the public from
U.S. Department of Commerce
National Technical Information Service
5285 Port Royal Road
Springfield, VA 22161
Telephone: (800) 553-6847
Facsimile: (703) 605-6900
E-mail: orders@ntis.fedworld.gov
Online ordering: <http://www.ntis.gov/ordering.htm>

OR

Lawrence Livermore National Laboratory
Technical Information Department's Digital Library
<http://www.llnl.gov/tid/Library.html>

A COMPARISON OF THE EFFECT OF TEMPERATURE ON THE PASSIVITY BREAKDOWN AND REPASSIVATION POTENTIALS OF WROUGHT AND WELDED ALLOY 22 IN 5 M CaCl₂

G. O. Ilevbare

Lawrence Livermore National Laboratory
7000 East Ave, L-631, Livermore CA 94550, USA

ABSTRACT

The study of the electrochemical behavior of wrought and welded Alloy 22 was carried out in 5 M CaCl₂ at various temperatures. Comparisons were made between the electrochemical behaviors of the wrought and welded forms of Alloy 22 Multiple Crevice Assembly (MCA) specimens. The susceptibility to corrosion was found to increase with increase in temperature in both the wrought and the welded forms of the alloy. Nevertheless, the measure critical breakdown potential E_{crit} was found to be similar for the wrought and welded specimens.

INTRODUCTION

Alloy 22 (N06022) is a nickel alloy rich in chromium and molybdenum, with a high degree of corrosion resistance. It exhibits a low general corrosion rate under most conditions and has formidable localized corrosion resistance in most environments compared with other nickel alloys [1-8]. Consequently, Alloy 22 has emerged as the leading candidate for the fabrication of high-level nuclear waste containers, containers that are intended for use for disposal of high-level radioactive waste and spent nuclear fuel. On July 23, 2002, The United States Congress approved the site at Yucca Mountain, Nevada, for development as a repository for disposal of these materials.

Since welding will be used to close the waste containers, it is important to fully characterize and understand the electrochemical behavior of the welds and the areas adjoining the welds. One way of doing this would be to compare the behavior of non-welded (wrought) Alloy 22 to that of a welded material to determine whether there is increased susceptibility to corrosion in the welded zones and areas adjacent to the welded zones.

The study of the effect of temperature on the corrosion properties of the alloy is important since during the projected 10,000-year service life, the containers will pass through a heat gradient produced by the nuclear reactions taking place in the waste. Temperatures will be high (above the boiling point of water) in the early service life of the containers, while lower temperatures will prevail much later due to radioactive decay. At this later stage, there is a possibility of ground water contacting the containers.

Highly concentrated chloride-only environments are not representative of Yucca Mountain environments. However, the effect of important individual anions (like Cl^-), which could impact the performance of the containers, must be understood. Crevice corrosion is a concern in Cl^- environments [2-4]. Consequently, the study of the crevice corrosion behavior of Alloy 22 in the wrought and welded forms has been carried out in 5 M CaCl_2 using a multiple crevice assembly (MCA) sample configuration. This configuration was optimized for the study of crevice corrosion as it provides 24 potential crevice generation sites on a surface area of less than 10 cm^2 . The temperature range of study was between 45 and $120 \text{ }^\circ\text{C}$.

EXPERIMENTAL PROCEDURE

The material used in this study is Alloy 22 (N06022). Alloy 22 samples were fabricated from wrought and welded plate specimens. The chemical composition as documented by the supplier appears in Table 1. The composition is consistent with ASTM-B 575 (for plates/sheets) standard [9, 10]. The Multiple Crevice Assembly (MCA) specimens look like lollipops [2]. The design was optimized for the study of crevice corrosion so that most of the working surface was covered by the crevice former. The working surfaces of the MCA samples were used in the as-received state after degreasing with acetone and methanol. In the as-received state, the working surfaces of the MCA samples were finished to a root mean square (RMS) roughness average (RA) of between 2 and 5 micro inches with an air formed oxide film. During fabrication, the MCA samples were cut with an electro discharge machine (EDM). The edge (surface 90 degrees in angle to the working surface) of the sample was therefore left with a much rougher surface finish (Figure 1). Owing to this, the character of the oxide film on the edge of the specimen might be different from that of the working surface. This edge was removed by polishing with 600-grit SiC paper on all the welded samples, as well as on all the wrought samples tested at $120 \text{ }^\circ\text{C}$, 4 of the 6 tested at $45 \text{ }^\circ\text{C}$, and 2 of the 6 tested at $60 \text{ }^\circ\text{C}$. All the wrought samples tested at 75 and $90 \text{ }^\circ\text{C}$ were not ground at the edges. Leaving the rough edge on some specimens enabled the study of the effect of the rough EDM finish edge on the electrochemical response of the samples. The welded MCA specimens were identical to the wrought specimens. The band of weld metal on the samples was co-axial with the hole in the middle of the specimen, and covered an area on working surface that was at least 1 cm wide and extended across the entire face of the specimen on which the crevice formers were assembled. The welds were made by gas tungsten arch welding (GTAW). The rest of the Multiple Crevice Assembly (MCA) consisted of Titanium (Ti) grade 2 nuts, bolts and washers, as well as ceramic crevice formers with multiple ridges. The bolts were polytetrafluoroethylene (PTFE) wrapped to prevent these hardware components from being in electrical contact with the specimen. Each crevice former had a total of 12 ridges on it, creating 12 different potential crevice sites on each face of the specimen, and a total of 24 potential sites in each assembly [2]. The assembly was tightened to a torque of 70 in-lb. PTFE tape inserts were placed between the ceramic crevice former and the MCA sample prior to tightening. This was done to fill in the micro voids created by the micro-rough surfaces of the sample and the ceramic crevice former, and to increase the reproducibility of the tight crevices in all samples. The total surface area of the MCA specimen immersed in the electrolyte was 7.43 cm^2 . This surface area included the area under the 24 ridges of the crevice formers,

which had a combined surface area of 1.6 cm^2 . In current density estimations, the surface area of 7.43 cm^2 was used for calculations.

A three-electrode cell with a capacity of 1000 cm^3 was used for experimentation. The volume of electrolyte in the cell was about 900 cm^3 . A saturated silver/silver chloride (SSC) (Ag/AgCl) electrode was the reference electrode (RE). The RE was maintained near room temperature by mounting it at the end of a Luggin probe, which had a water-cooled jacket around it. The temperature of the water pumped through the cooling jacket was about $12 \text{ }^\circ\text{C}$. Thermal liquid junction calculations showed that potential variation caused by this phenomenon was in the order of a few mV ($\sim 10 \text{ mV}$ maximum). Also, according to Macdonald et al., a high KCl concentration in the reference electrode tends to suppress thermal liquid junction potentials across the boundary between the high and low temperature solutions [11]. The liquid junction potential variations were therefore ignored in further analyses. The counter electrode was made of platinum (Pt) foil. The temperature of the electrolyte was maintained by means of an oil-filled heating bath. The sample was immersed into the cell after the electrolyte had attained the desired temperature. The temperature was taken before and after the experiment with a thermocouple immersed into the electrolyte. Electrochemical measurements were carried out using a potentiostat. The corrosion potential (E_{corr}) was monitored for 24 hours. This was followed by cyclic potentiodynamic polarization measurements immediately afterwards. Cyclic polarization was started approximately 100 mV below E_{corr} , and continued until the current density from the sample reached a maximum of up to 30 mAcm^{-2} , or a maximum of 1.3 V (SSC) before the scan was reversed. The sweep rate in the forward and reverse directions was 0.1667 mVs^{-1} (600 mVh^{-1}). Deaerated 5 M CaCl_2 with a pH-6 was used, at various temperatures in these experiments. Nitrogen gas (N_2) was bubbled through the electrolytes for at least one hour before and throughout the experiments at a rate of 100 cc per minute. All electrolytes were prepared using certified American Chemical Society (ACS) grade chemicals.

EXPERIMENTAL RESULTS

The Corrosion Potential (E_{corr})

Figure 2 shows a summary of the average E_{corr} values between $45 \text{ }^\circ\text{C}$ and $120 \text{ }^\circ\text{C}$ for wrought and welded samples of Alloy 22. The error bars in Figure 2 are the standard deviations of the distributions. Figure 2 shows that E_{corr} from the wrought and welded metals cannot be separated with confidence. There was a difference of approximately 60 mV between the highest and lowest average E_{corr} values recorded. E_{corr} does not seem to be affected by temperature on both the wrought and welded samples over the temperature range studied (Figure 2). The number of repeats which make the average values presented range from 2 to 8. In each experiment, E_{corr} was recorded at the end of the 24-hour period of the experiments, and used to compute the averages shown. The progress individual E_{corr} values did not follow a particular trend over the 24-hour period. On some samples, the E_{corr} stayed fairly constant, while on others, it either increased or decreased over the 24-hour period. This pattern was observed irrespective of the temperature and for both the wrought and the welded samples. These 24-hour E_{corr} transients are

insufficient to predict what trend the evolution of the E_{corr} over longer exposure periods of time will follow.

The Breakdown Potential (E_{crit})^a

Figures 3 and 4 show representative polarization curves at the extremes of the temperature range tested (45 and 120 °C) for the wrought and welded MCA samples. Both the wrought and the welded forms of Alloy 22 showed a similar behavior at the respective temperatures of 45 and 120 °C. In Figure 3, there is a drop in current density after an initial rise in current density at 45 °C. This drop in current density created an "anodic peak" or "hump" between -0.1 and 0.3 V_{SSC} . These current excursions could sometimes reach values of about 30 mAcm^{-2} . Upon the drop in current density, the metal attained a passive state. The current density in this passive region sometimes fell to or below initial passive current density levels attained before the positive current excursion in the hump, suggesting that a reasonably good passive film had been formed. With the exception of one (of six) wrought sample tested at 60 °C where the sample did not repassivate after the initial current excursion, this behavior was observed on all the samples tested at 45 and 60 °C on both the wrought and welded samples. It was observed on one specimen apiece on the wrought (1 of 6) and welded (1 of 2) at 75 °C. A further increase in potential from the passive region resulted in another increase in the current density, signifying a breakdown of the oxide film at potentials higher than 0.8 V_{SSC} at 45 °C. A reversal of the potential on for the reverse sweep of the polarization produced no hysteresis loop. The absence of a hysteresis loop is usually an indication of transpassive, rather than localized breakdown. The presence of the hump was not observed on any of the samples tested at 90 and 120 °C.

A summary of the breakdown potentials (E_{crit}) for both the wrought and the welded samples is presented in Figure 5. Two methods were used to determine E_{crit} . In the first method (Method 1), E_{crit} was the potential at which the threshold current density of $2 \times 10^{-5} \text{ Acm}^{-2}$ ($20 \text{ } \mu\text{Acm}^{-2}$)^b was attained. This threshold value is arbitrary, and was used only as a reference point as a basis for comparison of the data in this paper. It bears no other significance. As seen from Figure 2, Method 1 did not take into account the decrease in current density after the "hump" of the curves at 45 °C (and at 60 °C), nor the fact that at higher temperatures (60 to 90 °C) especially in the samples with edges that were not ground, the current density in the passive region was generally above the threshold current density. In the second method (Method 2), E_{crit} was taken as the potential that coincided with the onset of the first permanent rise in current density from the passive region. If the current density at the point of first permanent rise was less than $20 \text{ } \mu\text{Acm}^{-2}$, the potential was read at a point in the rise of the curve where the current density was at least $20 \text{ } \mu\text{Acm}^{-2}$. An asterisk (*) is used to denote the E_{crit} values obtained by Method 2.

^a "Critical breakdown potential", E_{crit} , as employed here is used to denote the potential(s) at which the breakdown of the passive film occurs by any type of corrosion attack such as pitting corrosion, crevice corrosion, general dissolution, or transpassive dissolution occurs.

^b At this current density, stable pitting or crevice corrosion would usually have commenced for various stainless steels, nickel and Alloy 22 [2-4, 7, 12-14].

Although the working surfaces of both the wrought and the welded samples were treated in the same way, the edges of the samples, which also contributed to the overall current density, were not. Therefore, the impact of this difference has to be understood before the data in Figure 5 can be properly assessed. Figures 6 and 7 show the differences in the electrochemical behavior (at 45 and 60 °C) between wrought samples that had their edges ground with 600-grit SiC paper and those that were not^c. It is clear from the curves in Figures 6 and 7 at 45 and 60 °C respectively that specimens which did not have their edges ground posted a higher anodic current density in the initial part of the anodic region extending up to the anodic peak or "hump". The difference in the current density at the anodic peak could be as high as 2 orders of magnitude in the "hump" as observed in Figure 7. The potential at which passivation occurs could also be more anodic for the sample which was not ground compared with one which was. The passive current density was usually slightly higher with the specimens that were not ground, but sometimes similar in magnitude as seen in Figure 7. Clearly, any comparison made between E_{crit} values of the wrought and welded specimens taken by Method 1 would be problematic. Nonetheless, E_{crit} values taken by Method 2 might not be so problematic because in samples at 45 and 60 °C that experienced drops in passive current densities after an initial current excursion (hump), the point of current increase is similar in both the ground and unground samples. This means that provided Method 2 is used, E_{crit} values obtained at 45 and 60 °C may be compared (Figures 6 and 7). A look at Figures 6 and 7 would also suggest that the crevice repassivation potential measured on the reverse sweep of the curves may be compared since they seem to be unaffected by the finish of the edge of the sample.

Figure 5 shows that the average value of E_{crit} falls with increase in temperature. The greatest difference in the value of E_{crit} occurred between 60 and 75 °C (Figure 5, Method 2). There is a convergence of the data taken by Methods 1 and 2 on the welded sample at 75 °C. The values of E_{crit} for the wrought and welded samples coincide at 120 °C. This shows that there is no difference in susceptibility to corrosion between the two types of specimen tested. Further analyses of the data showed that at 45 °C, the lowest temperature tested, comparing only the samples that had their edges ground with Method 1, E_{crit} was $0.121 \pm 0.011 V_{SSC}$ and $0.255 \pm 0.598 V_{SSC}$ for the wrought sample V_{SSC} for the welded sample, and from Method 2, were 0.924 ± 0.011 and $0.928 \pm 0.019 V_{SSC}$ respectively for the wrought and welded samples. At 60 °C, also comparing only the samples that had their edges ground by Method 1, the values for E_{crit} were $-0.143 \pm 0.083 V_{SSC}$ and $-0.205 \pm 0.107 V_{SSC}$ respectively for the wrought and welded samples. By Method 2, the values were $0.878 \pm 0.040 V_{SSC}$ and $0.765 \pm 0.112 V_{SSC}$ respectively for the wrought and welded samples. These values show that the E_{crit} for wrought and welded specimens were statistically similar and cannot be separated with confidence at 45, 60 and 120 °C (Figure 5). This suggests that the GTAW welds on the Alloy 22 specimens did not exhibit any adverse effect on the value of E_{crit} .

Crevice corrosion was observed at all temperatures on both the wrought and welded specimens. The degree of corrosion damage increased with increase in temperature. The crevices formed at 45 °C were the shallowest, and caused the least damage per unit area.

^c Recall that all welded samples had their edges ground but only wrought samples tested at 120; 4 of 6 at 45; and 2 of 6 at 60 °C were ground with 600-grit SiC paper. None of the wrought samples at 75 and 90 °C had their edges ground.

In the welded samples, crevice attack, although it occurred in the weld metal zones, seemed to be less severe than on the non-weld metal areas (Figures 8 and 9). In Figure 8 (75 °C; 5 M CaCl₂), the band of weld metal appears darker than the base metal in the top portion of the photo. The deepest crevices are located in the region of the base metal. Similarly, in Figure 9 (120 °C, 5 M CaCl₂), the deep crevices that formed in the lower base metal half of the image seem to terminate at the boundary of the base and weld metal. These images suggest that the weld metal is better able to resist localized attack in 5 M CaCl₂.

The Repassivation Potential (E_{rp})

The repassivation potential was taken as the potential that coincided with a current density of $20 \mu\text{Acm}^{-2}$ on the reverse sweep of the cyclic polarization curves. Figure 10 shows a summary of the repassivation potentials obtained from both the wrought and welded samples between 45 and 120 °C. On both the wrought and the welded samples, the repassivation potential E_{rp} decreased with increasing temperature. The values for the wrought and welded samples were also similar and cannot to be separated with confidence. Figure 11 shows E_{crit}^* , E_{rp} and E_{corr} for both the wrought and the welded samples. The values for E_{crit}^* and E_{rp} are close at 45, 60 and 120 °C. There is a difference of about 150 mV_{SSC} between E_{crit}^* and E_{rp} at 75 and 90 °C, with the value of E_{crit}^* being lower, except at 75 °C on the welded sample where E_{crit}^* is higher by about 150 mV_{SSC}.

DISCUSSION

Under the environmental conditions in Yucca Mountain, it is unlikely that waste containers fabricated from Alloy 22 will ever be in contact with solutions of a chloride-only composition. For this reason, 5 M CaCl₂ (10 M Cl⁻) must be regarded as a theoretical extreme environment. There is little possibility of 5 M CaCl₂ being present under normal real-life repository conditions in the absence of any other anions or oxyanions. Ground waters from Yucca Mountain contain an array of anions and oxyanions, which include NO₃⁻ and SO₄²⁻, which have been found to inhibit localized corrosion in stainless steels and nickel alloys [13-22]. Indeed, earlier work showed that Alloy 22 is not susceptible to localized corrosion in simulated concentrated solutions that are relevant to the repository ground water [1].

The similarity in the values of the E_{corr} for the wrought and the welded samples over the temperature range tested suggest that there will be difficulty in creating and sustaining viable galvanic couples which could lead to breakdown of the oxide film either on the base metal or weld (depending on which potential is higher). The reason for this is because the composition for the weld metal in the welded sample is similar to that of the base metal (Table 1).

The higher current densities exhibited by the samples, which did not have the EDM, finished edged removed by grinding might be due to a combination of two facts. From Figure 1, it can be seen that the EDM finished edge of the sample was rougher than the

working surface of the sample. This increased roughness would result in an increase of the surface area of the sample, which would in turn result in an increase in the current density calculated with a surface area assuming a fairly flat/smooth surface. However, this increase in surface area alone might not be sufficient to account for the high current densities observed. Another factor might be that the surface oxide in this region was more active than the rest of the sample because the oxide film has been altered by the EDM.

The similarities in the values of E_{crit} and E_{rp} of the wrought and welded versions of the samples are consistent with their similarities in composition (Table 1). However, images in Figure 8 and 9 suggest that the weld and base metal exhibit different propensities to crevice corrosion, with the welded metal able to better resist crevice corrosion. The similarities in the value of E_{crit} on both the welded and wrought samples might therefore reflect the E_{crit} of the wrought or base metal, rather than that of the weld metal. Since the propinquity of the E_{corr} values between the wrought and the welded samples suggest that powerful galvanic couples may not be viable, the greater susceptibility of the base compared with the weld metal is believed to be due to a metallurgical effect. However, the fact that both the weld and base metal are present on the same sample creates a difficulty in accurately acquiring the contribution of each metal type to the E_{corr} of the welded MCA samples. Nonetheless, although the E_{corr} of the welded sample is a composite of the E_{corr} of the weld and base metals, the propinquity of the E_{corr} of the wrought and welded samples strongly suggests that the E_{corr} of pure base metal (wrought) might be close to that of pure weld metal. Clearly, more work is required in this area to understand, and possibly isolate the main reason for the differences in susceptibility to localized corrosion.

The anodic peaks or "humps" exhibited by both the wrought and the welded versions of the sample at 45, 60, and sometimes at 75 °C is not fully understood. However, there is some difficulty in reactivating the sites of breakdown after passivation has occurred. This suggests that a good passive film forms on the metal surface after the initial current excursion. Transpassive dissolution usually results in the breakdown of the film after passivation. An observation of the samples tested at 45 and 60 °C showed the presence of both localized damage (which probably occurred at lower than the transpassive potential), and uniform damage due to transpassive dissolution at high potentials. The notion of transpassive breakdown is also supported by the almost identical breakdown potentials measured on both versions of the sample at 45 °C by Method 2. Clearly, further work is needed especially in the area of surface analyses to increase understanding of what is happening at current peak regions in the anodic scans.

CONCLUSIONS

1. Temperature (between 45 and 120 °C) has little or no effect on the E_{corr} of Alloy 22 on both the wrought and the welded samples.
2. E_{crit} is similar on both the wrought and welded samples in 5 M $CaCl_2$ between 45 and 120 °C, however the weld metal was found to be less susceptible to crevice attack compared with the base metal in the welded samples.

3. In 5 M CaCl₂ between 45 and 120 °C E_{crit} is shifted to lower potentials as temperature increased on both the wrought and the welded samples.
4. The repassivation potential is similar on both the wrought and welded samples in 5 M CaCl₂ between 45 and 120 °C.

REFERENCES

1. G.O. Ilevbare T. Lian and J.C. Farmer, Environmental Considerations in the Studies of Corrosion Resistant Alloys for High-Level Radioactive Waste Containment Paper No. 02539, Corrosion 2002.
2. G.O. Ilevbare, Electrochemical Behavior of Alloy 22 in 5 M CaCl₂, Transportation Storage, and Disposal of Radioactive Materials, PVP-Vol. 449, p.55 2002. American Society of Mechanical Engineers (ASME), New York, USA.
3. B. A. Kehler, G.O. Ilevbare and J.R. Scully Corrosion, 57, pp. 1042, 2001.
4. B. A. Kehler, G. O. Ilevbare and J. R. Scully Corrosion 2001, Crevice Corrosion Behavior, of Ni-Cr-Mo Alloys: Comparison of Alloys 625 and 22, NACE Topical Research Symposium, p.30, March 2001.
5. Haynes International, Inc., Product Brochure H-2019E, Haynes International Inc. Kokomo, IN, p.22, 1997.
6. J. C. Farmer, D. McCright, G.E. Gdowski, F. Fang, T. Summers, P. Bedrossian, J. Horn, T. Lian, J. Estill, A. Lingenfelter, and W. Halsey, General and Localized Corrosion of Outer Barrier of High-Level Waste Container in Yucca Mountain, May 2000. Preprint UCRL-JC-138890, Lawrence Livermore National Laboratory, Technical Information Department Digital Library.
7. K.A. Gruss, G.A. Cragnolino, D.S. Dunn and N.Sridhar, Corrosion '98, Paper No. 149, 1998.
8. S.J. Lukezich, The Corrosion Behavior of Ni-Base High Performance Alloys in Simulated Repository Environments, MS Thesis, The Ohio State University 1989.
9. ASTM B574, Annual Book of ASTM Standards, Nonferrous Metal Products, Volume 02.04, p.531, American Society of Testing and Materials, West Conshohocken, PA (2000).
10. ASTM B575, Annual Book of ASTM Standards, Nonferrous Metal Products, Volume 02.04, p.535, American Society of Testing and Materials, West Conshohocken, PA (2000).
11. D.D. Macdonald, A.C. Scott, and P. Wentreck, J. Electrochem. Soc., **126**, 908 (1978).
12. N.D. Rosenberg, G.E. Gdowski, and K.G. Knauss, Applied Geochemistry, 2001. **16**: p.1231.
13. R.C. Newman and T. Shahrabi, Corrosion Science, 1987. **27**: p.827.
14. H. Yashiro and K. Tanno, Corrosion Science, 1990. **31**: p. 485.
15. H.H Uhlig and J.R. Gilman, Corrosion, **20**, 289t (1964).
16. H. P. Leckie and H.H. Uhlig, J. Electrochem. Soc., **117**, 1152 (1966).
17. I.L. Rozenfeld, and I.S Danilov, Corrosion Science, **7**, 129 (1967).
18. E.A. Lizlovs and A.P. Bond, J. Electrochem Soc., **116**, 574 (1969).
19. Z. Szklarska-Smialowska, Corrosion Science, **11**, 209 (1971).

20. Z. Ahmed, Corrosion, **33**, 161 (1977).
21. H.H. Strehblow, and B. Titze, Corrosion Science, **17**, 461 (1977).
22. H.C. Man and D. R. Gabe, Corrosion Science, **21**, 713 (1981).

Acknowledgements

The Department of Energy Office of Civilian Radioactive Waste Management (OCRWM) sponsored this work. This work was done under the auspices of the U.S. Department of Energy (DOE) by the University of California, Lawrence Livermore National Laboratory (LLNL) under contract No. W-7405-Eng-48. This work is supported by Yucca Mountain Site Characterization Project, LLNL.

Table 1. Chemical composition of Alloy 22 (UNS No. N06022) given in weight percent.

| Element | Actual Composition | | | ASTM Requirements ASTM B575-Sheets |
|---------|--------------------|-------------------------------|------------------------|---------------------------------------|
| | Wrought | Welded (Weld/Filler Metal) | Welded (Base Metal) | |
| Mo | 14.10 | 14.00 | 13.82 | 12.5-14.5 |
| Cr | 22.00 | 20.54 | 20.38 | 20.0-22.5 |
| Fe | 4.50 | 2.08 | 2.85 | 2.0-6.0 |
| W | 2.70 | 3.10 | 2.64 | 2.5-3.5 |
| Co | 1.30 | 0.03 | 0.01 | 0.0-2.5 |
| C | 0.003 | 0.004 | 0.005 | 0.000-0.015 |
| Si | 0.03 | 0.06 | 0.05 | 0.00-0.08 |
| Mn | 0.31 | 0.20 | 0.16 | 0.00-0.50 |
| V | 0.16 | 0.03 | 0.171 | 0.00-0.35 |
| P | 0.01 | 0.004 | 0.008 | 0.00-0.02 |
| S | <0.01 | 0.001 | 0.0002 | 0.00-0.02 |
| Ni | Bal. | Bal. | Bal | Bal. |

Wrought Specimens from Heat # 2277-5-3203. Welded Specimens: Base metal from Heat #059902LL1; Weld/filler metal from Heat # XX1753BG.

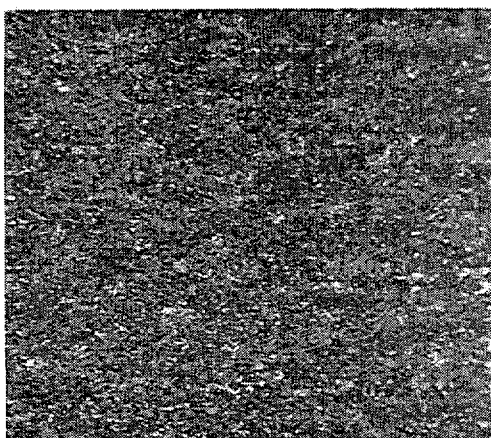


Figure 1a: The EDM surface finish on the edge of the sample at a magnification of x30.

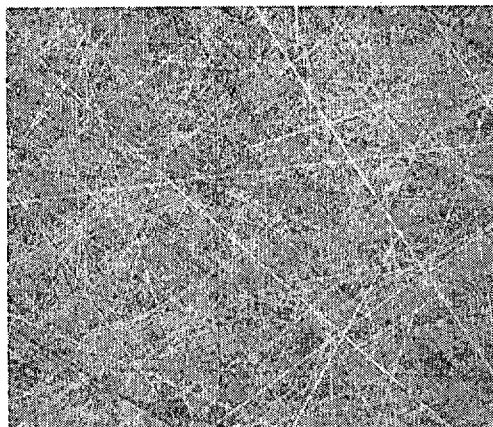


Figure 1b. The surface finish on the working surface and the face of the stem on the MCA sample at a magnification of x30. This is an RMS finish of between 2 and 5 micro inches roughness average.

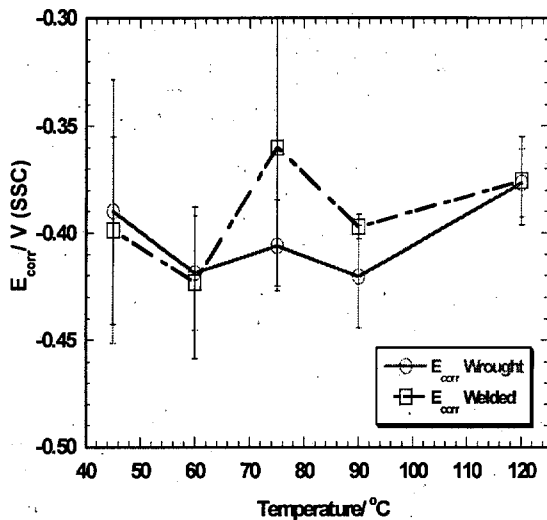


Figure 2. E_{corr} as a function of temperature on wrought and welded MCA samples in 5 M $CaCl_2$.

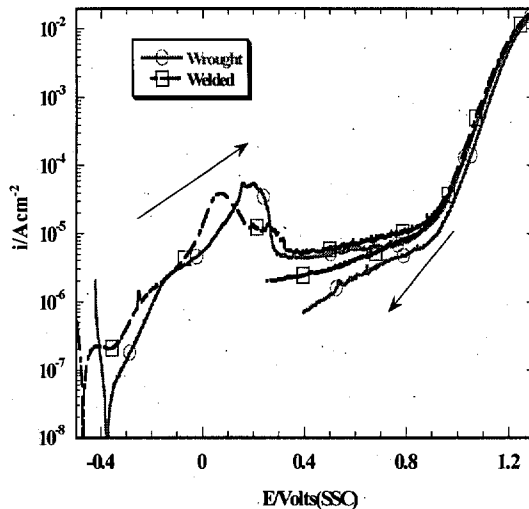


Figure 3: Polarization curves of wrought and welded MCA samples in 5 M $CaCl_2$ at 45 °C. Both samples had their edges ground with 600 Grit SiC paper. Sweep rate, 0.1667mV/s

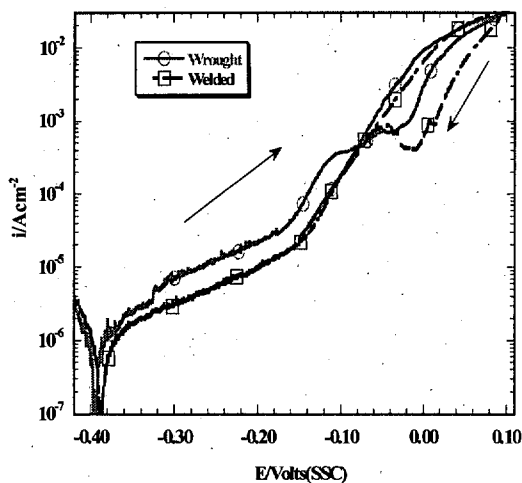


Figure 4: Polarization curves of wrought and welded MCA samples in 5 M $CaCl_2$ at 120 °C. Both samples had their edges ground with 600 Grit SiC paper. Sweep rate, 0.1667mV/s

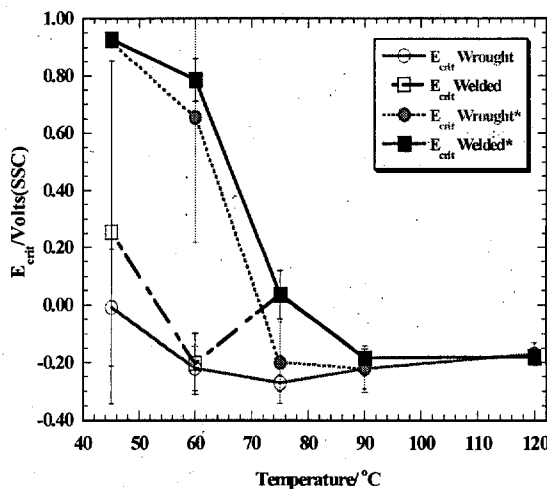


Figure 5. Average E_{crit} as a function of temperature on wrought and welded MCA Alloy 22 samples in 5 M $CaCl_2$. (*) Denotes the measurements taken using Method 2.

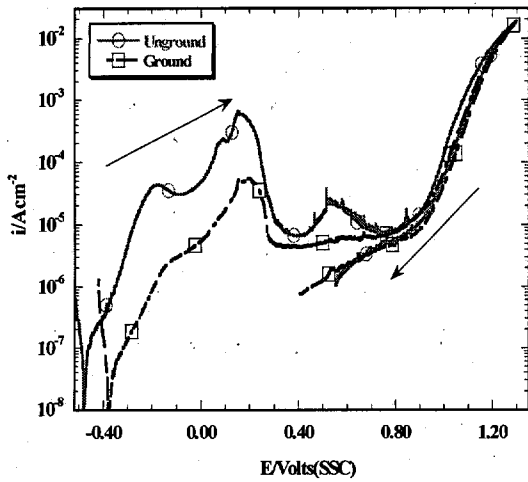


Figure 6. Polarization curves in 5 M CaCl_2 comparing a wrought sample with ground edges with one with edges with were not ground. Temperature: 45 °C.

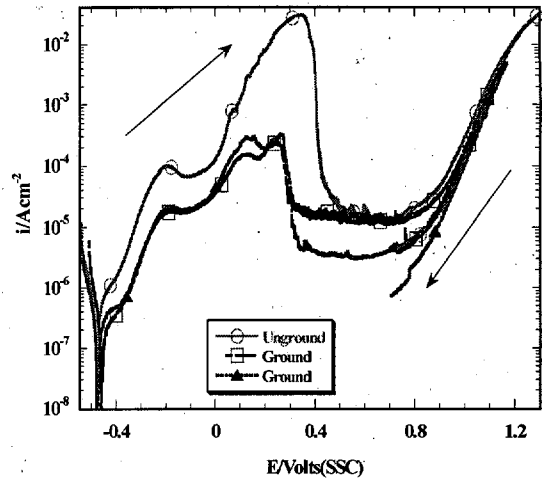


Figure 7. Polarization curves in 5 M CaCl_2 comparing a wrought sample with ground edges with one with edges with were not ground. Temperature: 60 °C.

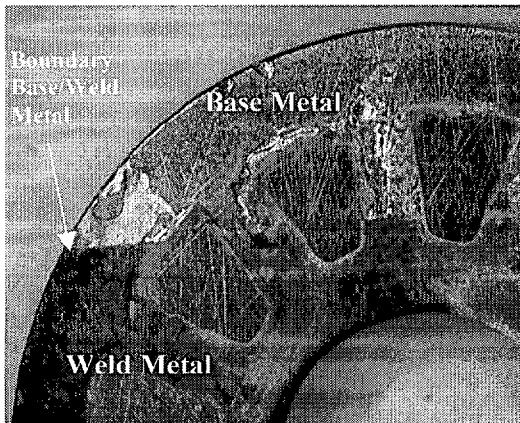


Figure 8. Welded MCA after 24 hours at E_{corr} , and cyclic polarization in 5 M CaCl_2 at 75 °C.

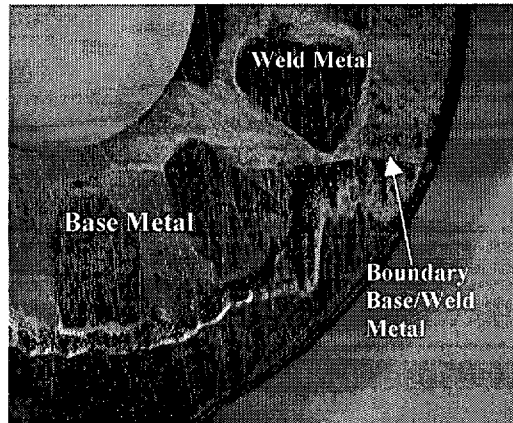


Figure 9. Welded MCA after 24 hours at E_{corr} , and cyclic polarization in 5 M CaCl_2 at 120 °C.

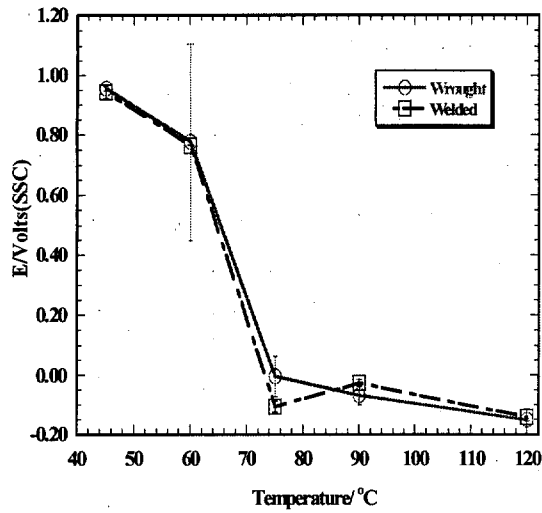


Figure 10. Average E_{tp} as a function of temperature on wrought and welded MCA Alloy 22 specimens in 5 M CaCl_2 .

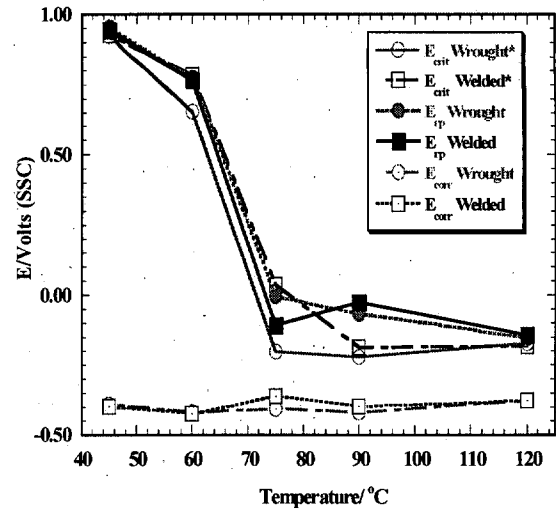


Figure 11. Average E_{crit} , E_{tp} and E_{corr} as a function of temperature of wrought and welded MCA Alloy 22 specimens in 5 M CaCl_2 .